analytical chemistry

pubs.acs.org/ac Article

^{1}D-Guided Differential Rescaling of a Contour Plot in Comprehensive 2D Gas Chromatography

Wenzhe Zang, Xiaheng Huang, Ruchi Sharma, and Xudong Fan*

Cite This: *Anal. Chem.* 2024, 96, 3960−3969 Read Online

ACCESS | Metrics & More | Article Recommendations | Supporting Information

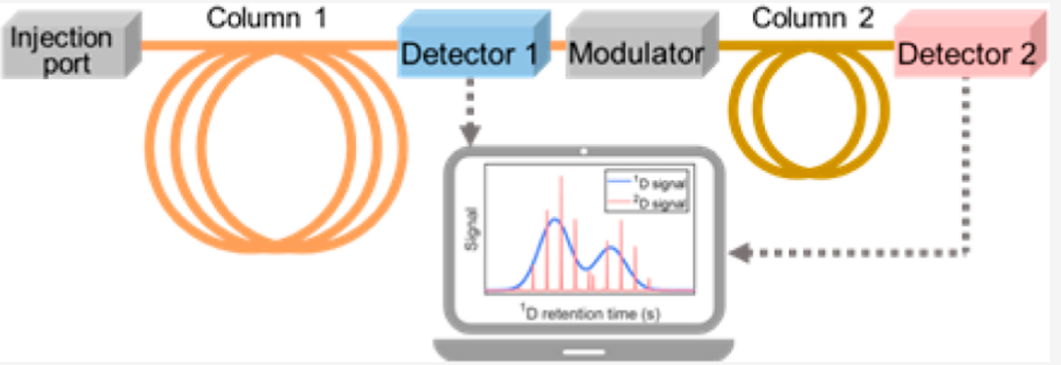

ABSTRACT: A ^{1}D-guided differential rescaling algorithm for a contour plot is developed based on our recently proposed comprehensive two-dimensional gas chromatography (GC × GC) system with a first-dimensional (^{1}D) detector added. Chromatograms obtained from ^{1}D and second-dimensional (^{2}D) detectors are both incorporated during the data processing. As compared to the conventional contour plot methods using only ^{2}D data, our algorithm can significantly improve precision and consistency of GC × GC results in terms of retention times, peak widths, and peak areas or volumes, regardless of modulation time selection, modulation phase shift fluctuations, and modulation duty cycle. The peak identification, quantification, and capacity can therefore be enhanced. Furthermore, the ^{1}D-guided differential rescaling method is shown to better handle the coelution and missing peak issues often encountered in the conventional methods. Finally, the new method exhibits high versatility in ^{1}D and ^{2}D detector selection, which greatly broadens GC × GC utility. Our method can easily be adapted to other two-dimensional chromatography systems that have direct access to ^{1}D chromatograms.

INTRODUCTION

Comprehensive two-dimensional gas chromatography (GC × GC, Figure 1A) uses two columns of different stationary phases so that vapor analytes are subjected to two independent separations to achieve a peak capacity higher than the corresponding one-dimensional GC.[1−6] A modulator is placed between the first-dimensional (^{1}D) and second-dimensional (^{2}D) columns and periodically sends a portion of the ^{1}D effluent to the ^{2}D column. Usually, a pneumatic modulator or thermal modulator is used to achieve so-called snapshot modulation or accumulative modulation.[7,8]

In a conventional GC × GC (Figure 1A), only a ^{2}D detector is used at the end of the ^{2}D column to detect the effluents coming out of the system. A two-dimensional (2D) chromatogram (*i.e.*, contour plot) is constructed by using the ^{2}D chromatograms sequentially measured by the ^{2}D detector. ^{1}D information (such as retention time $^{1}t_{r}$, peak profiles, and intensities) can only be indirectly extracted from the ^{2}D data (along with the timing information provided by the modulator). There are a few major drawbacks in the conventional GC × GC. First, there is a dilemma in modulation time, P_{M}.[6,9,10] On one hand, accurate reconstruction of ^{1}D peaks requires a shorter P_{M}. On the other hand, ^{2}D separation prefers to have a longer P_{M} to improve ^{2}D separation and avoid a potential wrap-around issue. A long P_{M} (*i.e.*, a low ^{1}D sampling rate) often results in distorted peak profiles, additional peak broadening, inaccurate peak retention times, and missing peaks in ^{1}D, which in turn reduces the overall peak capacity for GC × GC and adversely affects peak identification and quantification.[8,11] The modulation time dilemma exacerbates when asymmetric peaks (tailing or fronting) and/or narrower peaks are present in ^{1}D, and when the analyte quantity is so low that may not be detectable by the ^{2}D detector.[6,10,12,13] In addition, the normal random-

Received: January 10, 2024
Revised: February 7, 2024
Accepted: February 8, 2024
Published: February 22, 2024

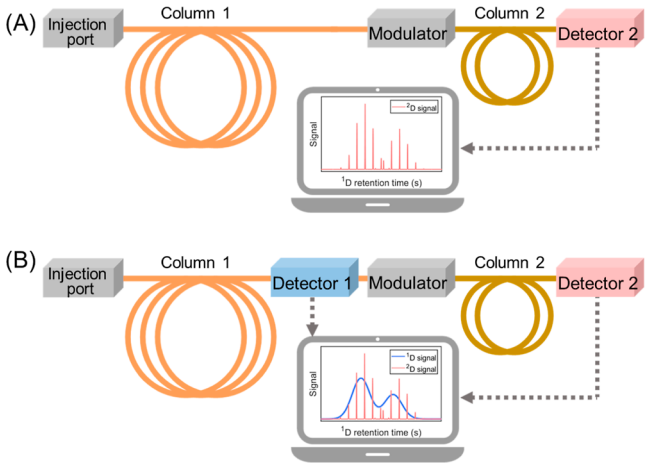

Figure 1. (A) Conventional comprehensive two-dimensional GC (GC × GC) configuration, where only a ^{2}D detector (pink) is used at the end of the ^{2}D column. (B) New GC × GC configuration, where an additional ^{1}D detector (blue) is used at the end of the ^{1}D column.

ness of modulation timing produces varied displays of ^{2}D peaks (*i.e.*, varied intensities and ^{1}D timing of the ^{2}D slices), and hence alters the reconstructed contour profiles (position, shape, and amplitude) from run to run. This further affects the precision, reproducibility, and reliability in 2D contour plots, especially the information projected along ^{1}D.

Marriott and his coworkers have been pioneering in improving the precision of ^{1}D information extraction based on the conventional GC × GC setup. Experimental efforts included mapping out a series of GC × GC analyses by varying the start time of the modulator (*i.e.*, only varying the phase shift, whereas other conditions remain the same).[6] Theoretically, this approach is likely to obtain the true peak maximum (*i.e.*, ^1t_r) and peak area in ^{1}D. However, practical implementation is very challenging due to the substantially prolonged turn-around time, inaccurate control of phase shift, and fluctuations in other chromatographic conditions such as ambient temperature, and flow rate, *etc.* Recently, the same team introduced a novel data processing approach based on conventional GC × GC with mass spectrometry (MS) to improve compound identification.[14] The workflow involves curve-fitting and considering modulation phase shift. Improvement in resolution and reproducibility was successfully demonstrated. However, this method relies heavily on a precise control of phase shift, which is infeasible for many exiting modulators. Prior knowledge of the number of peaks is also needed from MS data, which limits its application for the detectors without identification capabilities. Additionally, use of various fitting techniques that depend on peak profiles complicates automation in data analysis and could impair its performance in the presence of narrow peaks that disallow for sufficient modulation events.

Instead of relying solely on ^{2}D data, one intuitive way, and probably the only precise way, to obtain the true ^{1}D information is to add a ^{1}D detector at the ^{1}D column outlet to probe effluents before they enter a modulator (Figure 1B). This configuration has several advantages. First, the ^{1}D information can be obtained directly from the ^{1}D detector with a much higher ^{1}D sampling rate (equal to data acquisition frequency of the ^{1}D detector), instead of being indirectly reconstructed from the ^{2}D (sampling rate is equal to modulation frequency $1/P_M$). The ^1t_r peak profile, and intensity along ^{1}D can be precisely and reliably extracted regardless of modulation time selections and phase shift fluctuations. Second, peak capacity ($n_c = {}^1n_c \times {}^2n_c$) of GC × GC can be improved. In conventional GC × GC, ^1n_c is extracted from the ^{2}D chromatogram and can be deteriorated due to insufficient modulation frequency (or ^{1}D sampling rate). Finally, it improves precisions for trace compounds analysis when analytes can be picked by the ^{1}D detector but fail at the ^{2}D detector after several times of modulations. All these result in more reliable and reproducible resolution, identification, and quantifications of analytes in GC × GC.

For the proposed configuration, the requirements for such a ^{1}D detector are as follows: (1) non- or minimally destructive to the analytes and (2) introducing negligible extra band broadening (*i.e.*, zero dead volume). Unqualified detector examples include MS, flame ionization detector (FID), and conventional thermionic ionization detector (TID). In contrast, the microfluidic photoionization detector (μPID) previously developed by our group[15,16] serves as a desired candidate for this role.

In our hardware work,[17,18] we have demonstrated the feasibility of adding a μPID at the end of the ^{1}D column in GC × GC systems. Meanwhile, we have also introduced a curve-fitting based method in an attempt to incorporate the information obtained by both ^{1}D and ^{2}D detectors.[17] However, some guess work and curve-fitting for various case enumerations are involved in the previous algorithm, which compromises its reliability when there are serious coelutions and thus hinders its applicability. Here, we propose a completely new method, the ^{1}D-guided differential rescaling (abbreviated as ^{1}D-DR) method, which eliminates the aforementioned guess work and curve-fitting process. The algorithm developed here makes full use of the ^{1}D and ^{2}D information and is broadly applicable to various 2D systems (such as GC × GC and LC × LC). In the following sections, the theory and algorithm will be first discussed, followed by systematic evaluation of the performance related to modulation times, modulation phase fluctuations, modulation duty cycles, and ^{1}D/^{2}D detector responsivities. Data generated both artificially and experimentally will be utilized for verification and discussion.

THEORY AND ALGORITHM DESCRIPTION

We start by briefly describing the conventional procedures (Figure 2A) to obtain a 2D chromatogram (contour plot) using a conventional GC × GC configuration (Figure 1A).

Step 1 (Conventional). Stack modulated ^{2}D chromatogram slices (*i.e.*, those obtained from the ^{2}D detector) sequentially side-by-side along the ^{1}D time axis. The modulated ^{2}D chromatogram slices are depicted on the major grids in red in Figure 2A. The distance between the neighboring major grids is equal to the modulation time (P_M).

Step 2 (Conventional). More ^{2}D chromatogram slices are generated through data interpolation based on the neighboring modulated ^{2}D chromatograms and are stacked along the ^{1}D axis. The interpolated ^{2}D chromatograms are plotted on the minor grids in black dashed lines in Figure 2A. The distance between the neighboring minor grids depends on the data interpolation density, which is usually chosen arbitrarily. In this work, we use 0.01 s so as to compare the conventional method with the ^{1}D-DR method.

Five different interpolation methods were recently compared by Allen and Rutan,[19] showing nearly equal performance. In

https://doi.org/10.1021/acs.analchem.4c00202
Anal. Chem. 2024, 96, 3960−3969

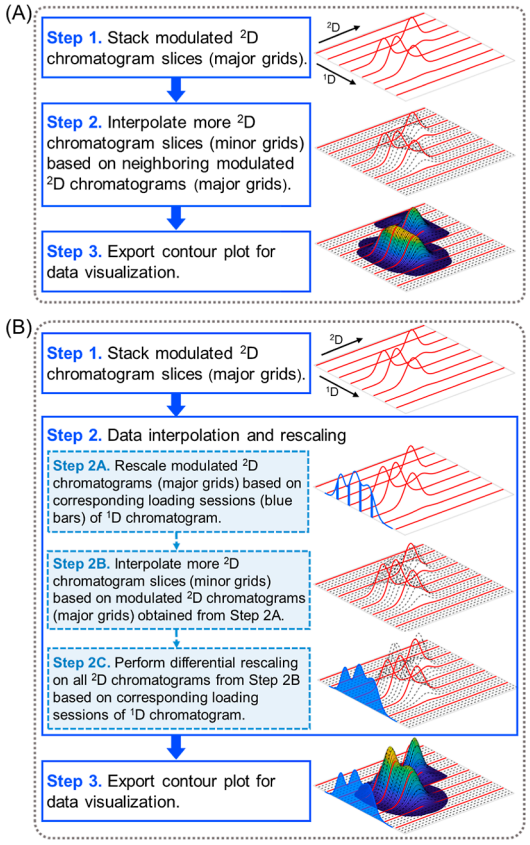

Figure 2. (A) Conventional method to obtain a 2D chromatogram (contour plot). (B) ^{1}D-DR method to obtain a 2D chromatogram (contour plot). Red solid lines: major grids. Black dashed lines: minor grids.

the current work, the modified Akima piecewise cubic Hermite interpolation[20] (Makima for short) as implemented in the "interp2" command in MATLAB was used to avoid the overshooting problem found in spline fitting.

Step 3 (Conventional). Merge all ^{2}D chromatograms (both modulated ones on the major grids and interpolated ones on the minor grids) and export a contour plot for data visualization.

As can be seen from above, the direct input of conventional method is a limited number of discrete snapshots (often 1−4 per peak) with a relatively large interval determined by P_M (Figure 2A, step 1). To obtain a visually continuous contour plot, significantly more data are generated to enrich the gaps between the modulations (*i.e.*, between the adjacent major grids). Conventionally, these newly generated data can only be predicted through mathematical interpolation, which is mostly monotonical, between neighboring ^{2}D chromatograms on major grids (Figure 2A, step 2). However, the evolution of the ^{1}D effluent from one modulation to the next is often nonmonotonical or is at varied slopes of change. The deviations between the true ^{1}D effluent evolution and that predicted *via* interpolation fundamentally account for the reduced precisions of ^{1}D information in the conventional method.

In contrast to the conventional method described above, adding a ^{1}D detector in GC × GC (Figure 1B) allows us to obtain nearly continuous ^{1}D chromatogram [$^1S(t)$]. Therefore, on top of the interpolation described above, the access to $^1S(t)$ contributes an additional confinement to all ^{2}D chromatograms [$^2S(t)$]. That is, $^2S(t)$ should not be interpolated "arbitrarily" in the conventional method, rather it needs to be "reshaped" by $^1S(t)$. Figure 2B describes the workflow of our ^{1}D-DR method for the GC × GC configuration in Figure 1B and how to use $^1S(t)$ to confine or reshape $^2S(t)$. Similar to the conventional procedures, there are three major steps involved. Step 1 is to stack modulated ^{2}D chromatograms along the ^{1}D time axis as the major grids. Steps 2 and 3 are to interpolate data and export a contour plot. The major difference between our method and the conventional one is in step 2, where areas of all stacked ^{2}D chromatograms (on both major grids and minor grids) are rescaled based on the area under the ^{1}D chromatogram during the corresponding loading session (*i.e.*, ^{1}D-guided rescaling).

The details of our ^{1}D-DR method are described as follows (Figure 2B).

> **Step 1 (^{1}D-DR)** is the same as step 1 in the conventional procedures.
> **Step 2 (^{1}D-DR).** Data interpolation and rescaling.
> **Step 2A** is to rescale the modulated ^{2}D chromatograms based on the ^{1}D chromatogram.

Due to mass conservation, each modulated ^{2}D chromatogram (red major grid in Figure 2B) is produced by part of $^1S(t)$ loaded into the ^{2}D column in a modulation period. Therefore, for a ^{2}D chromatogram, $^2S_n(t)$, on a red major grid at t_n, where t_n is the start time of the nth modulation event, the total quantity of the analytes loaded into the ^{2}D column is proportional to the area under $^1S(t)$ measured by the ^{1}D detector, within this modulation period, *i.e.*

$$^1A_n = \int_{t_n}^{t_n+t_L} {}^1S(t)\,\mathrm{d}t \tag{1}$$

where t_L is the ^{1}D-to-^{2}D loading time. $0 < t_L < P_M$ for modulators with a duty cycle of <1 (*e.g.*, most pneumatic modulators) and $t_L = P_M$ for ones with a 100% duty cycle (*e.g.*, most thermal modulators). Similarly, assuming no wrap-around issue in ^{2}D separation, the total quantity of analytes detected by the ^{2}D detector should be proportional to the total area under $^2S_n(t)$, *i.e.*

$$^2A_n = \int_0^{P_M} {}^2S_n(t)\,\mathrm{d}t \tag{2}$$

where $^2S_n(t)$ is the ^{2}D chromatogram measured by the ^{2}D detector during the nth modulation period. A rescaling factor, R_n, for this modulation period can be obtained as

$$R_n = \frac{^1A_n}{^2A_n} \tag{3}$$

Due to mass conservation, $^2S_n(t)$ for this modulation can be rescaled to

$$^2S_n'(t) = R_n \times {}^2S_n(t) \tag{4}$$

where $^2S_n'$ is the rescaled ^{2}D chromatogram.

Step 2B is to interpolate more ^{2}D chromatograms along the ^{1}D time axis using the rescaled ^{2}D slices ($^2S_n'$) obtained from step 2A. As illustrated in Figure 2B, these rescaled ^{2}D chromatograms are depicted on the major grids (red solid lines) with a time interval of P_M. The interpolated ones are depicted on the minor grids (black dashed lines), with an interval equal to data acquisition time of the ^{1}D detector ($^1\tau = 1/^1f$ seconds for ^1f Hz ^{1}D data acquisition frequency). Note

https://doi.org/10.1021/acs.analchem.4c00202
Anal. Chem. 2024, 96, 3960−3969

that ${}^1\tau$ should be much smaller than the P_M, since ${}^1\tau$ is generally well below 1 s (${}^1\tau$ = 0.01 s in this work) whereas P_M is usually on the order of several seconds. For the sake of convenience, we use the Makima interpolation in this work as described previously, though any interpolation method should work. Note that this step is similar to step 2 in the conventional method, except that the modulated ^{2}D chromatograms (on the major grids) that have been rescaled using ^{1}D data in step 2A (${}^2S_n'$) are used for interpolation instead of the original modulated ones (${}^2S_n$).

As a result, a series of ^{2}D chromatograms (on both major grids and minor grids), ${}^2E_k(t)$, are obtained and each grid is ${}^1\tau$ apart, where k represents the kth grid that has a ^{1}D time stamp of $k\cdot{}^1\tau$.

Step 2C is to rescale all ^{2}D chromatograms from step 2B [${}^2E_k(t)$] based on the ^{1}D chromatogram. Under the similar logic of step 2A, each ^{2}D chromatogram on a major or minor grid is supposed to be produced by a corresponding slice of the ^{1}D chromatogram loaded into the ^{2}D column. However, except those on the major grids, which are obtained from the ^{2}D detector and have been rescaled in step 2A, all ^{2}D chromatograms on the minor grids are produced by interpolation in step 2B. Therefore, we need to rescale all ^{2}D chromatograms using the ^{1}D chromatogram as guidance. This way is equivalent to creating a series of virtual ^{2}D injections with a pseudoloading time ($t_{L,pseudo}$) and a pseudomodulation time of ${}^1\tau$.

We can apply the same technique introduced in step 2A to all ^{2}D chromatograms.

$$ {}^1A_k = \int_{t_k}^{t_k + t_{L,pseudo}} {}^1S(t)\,\mathrm{d}t \tag{5} $$

where $t_{r,k} = k\cdot{}^1\tau$, is the kth grid (major and minor grids are counted together).

$$ {}^2A_k = \int_0^{P_M} {}^2E_k(t)\,\mathrm{d}t \tag{6} $$

Note that eq 6 is the same as eq 2, except that ${}^2E_k(t)$ includes the chromatograms on both major and minor grids. Accordingly, ${}^2E_k(t)$ for the kth grid can be rescaled to

$$ {}^2E_k'(t) = R_k \times {}^2E_k(t) \tag{7} $$

where R_k is

$$ R_k = \frac{{}^1A_k}{{}^2A_k} \tag{8} $$

For pneumatic modulators (duty cycle $\ll$ 1), where generally $t_L \ll P_M < {}^1W_{1/2}$ (peak width at half-maximum in ^{1}D), $t_{L,pseudo}$ can be set to be t_L, which is the case for all examples presented in section "Results and Discussion—Influence of Modulation Time and Phase Shift, Coelution, and Versatility in Detector Responsivity". However, for thermal modulators, the duty cycle is close or equal to 1 (*i.e.*, $t_L = P_M$). We can still set $t_{L,pseudo}$ to be t_L, which can still yield excellent consistency and accurate extraction of ${}^1t_r$. However, the resolution (*i.e.*, the reconstructed ^{1}D peak width using our method) might not be satisfactory, especially when $t_L = P_M$ is comparable to actual ^{1}D peak widths or to the distance between the neighboring coeluted peaks. In this case, we suggest setting $t_{L,pseudo}$ to be a much smaller value to improve the resolution. Detailed discussions can be found in section "Results and Discussion—Duty Cycle". Note that the major grids that have been rescaled in step 2A may also be rescaled once more in step 2C, since t_L in eq 1 of step 2A may be different from $t_{L,pseudo}$ in eq 5 of step 2C.

It is worth emphasizing that for each round of rescaling (step 2A and 2C), only the total area under the ^{2}D chromatograms (major grids in step 2A, and both major and minor grids in step 2C) are changed. In other words, only the intensity ordinates of ^{2}D chromatogram data points are rescaled whereas the abscissas (^{2}D time axis) remain the same. The chromatogram profiles (*e.g.*, the peak number, peak width, symmetry, ${}^2t_r$, and relative peak height among different peaks in each ^{2}D chromatogram slice) are preserved. It is highly recommended to correct the potential issues of major grids (*e.g.*, peak height reduced due to mass loss in the modulator) first to accurately anchor the subsequent interpolation in step 2B. Therefore, we do not suggest deferring the rescaling in step 2A to step 2C; the two rescaling procedures in step 2A and step 2C should be carried out separately. To further help understand step 2C in our ^{1}D-DR method and why we used the name "^{1}D-DR", we add an illustration in Figure S1.

Step 3 (^{1}D-DR) is the same as step 2 in the conventional procedure, which is to merge all as-obtained ^{2}D chromatograms and export a contour plot for data visualization.

EXPERIMENTS

Artificial Peak Generation. An in-house MATLAB program is used to generate the sampled Gaussian and exponentially modified Gaussian (EMG) peaks in ^{1}D with known elution times, peak standard deviations (*i.e.*, peak width), peak areas, and data acquisition frequency (100 Hz or ${}^1\tau$ = 0.01 s). The ^{2}D peaks are also generated using Gaussian functions with different modulation times (P_M), phase shifts, and different ^{1}D and ^{2}D detector responsivity ratios. ^{1}D-to-^{2}D loading periodically starts at $\varphi + P_M \times n$, (n = 0, 1, 2, 3, ...). φ ($<P_M$) is the phase shift within a modulation period P_M and describes the relative positions of the modulation events with respect to the position of a ^{1}D chromatographic peak (or band). The elution time along ^{1}D and ^{2}D is arbitrarily chosen and does not affect the conclusion. The features of the generated peaks are discussed in detail in section "Results and Discussion".

Experimental Data. Experimental chromatograms are generated on a portable comprehensive 2D μGC system constructed in-house, which consists of a DB-1 ms commercial column from Agilent J&W (nonpolar, length 10 m, i.d. 250 μm, film thickness 0.25 μm, P/N: 122-0162), a WAX coated ^{2}D microfabricated column (polar, length 0.5 m, cross section: 250 μm × 250 μm), a microfabricated flow-restricted pneumatic modulator, a helium cartridge (for carrier gas), and two flow-through μPIDs at the ^{1}D and ^{2}D outlets, respectively. The current 2D μGC device is very similar to the one reported in ref 18, except that the microfabricated ^{1}D column in ref 18 is now replaced by a commercial column. A breath sample from a lab member is collected as the model system. During the chromatographic separation, the helium flow rate is 2 mL/min in the ^{1}D column, column temperature is kept at 25 °C for 2 min, then first ramped to 80 °C at a rate of 10 °C/min, and next ramped to 120 °C at a rate of 40 °C/min. The operation on breath sampling and ^{1}D separation is the same as reported in our previous work.[21,22] The settings on

https://doi.org/10.1021/acs.analchem.4c00202
Anal. Chem. 2024, 96, 3960−3969

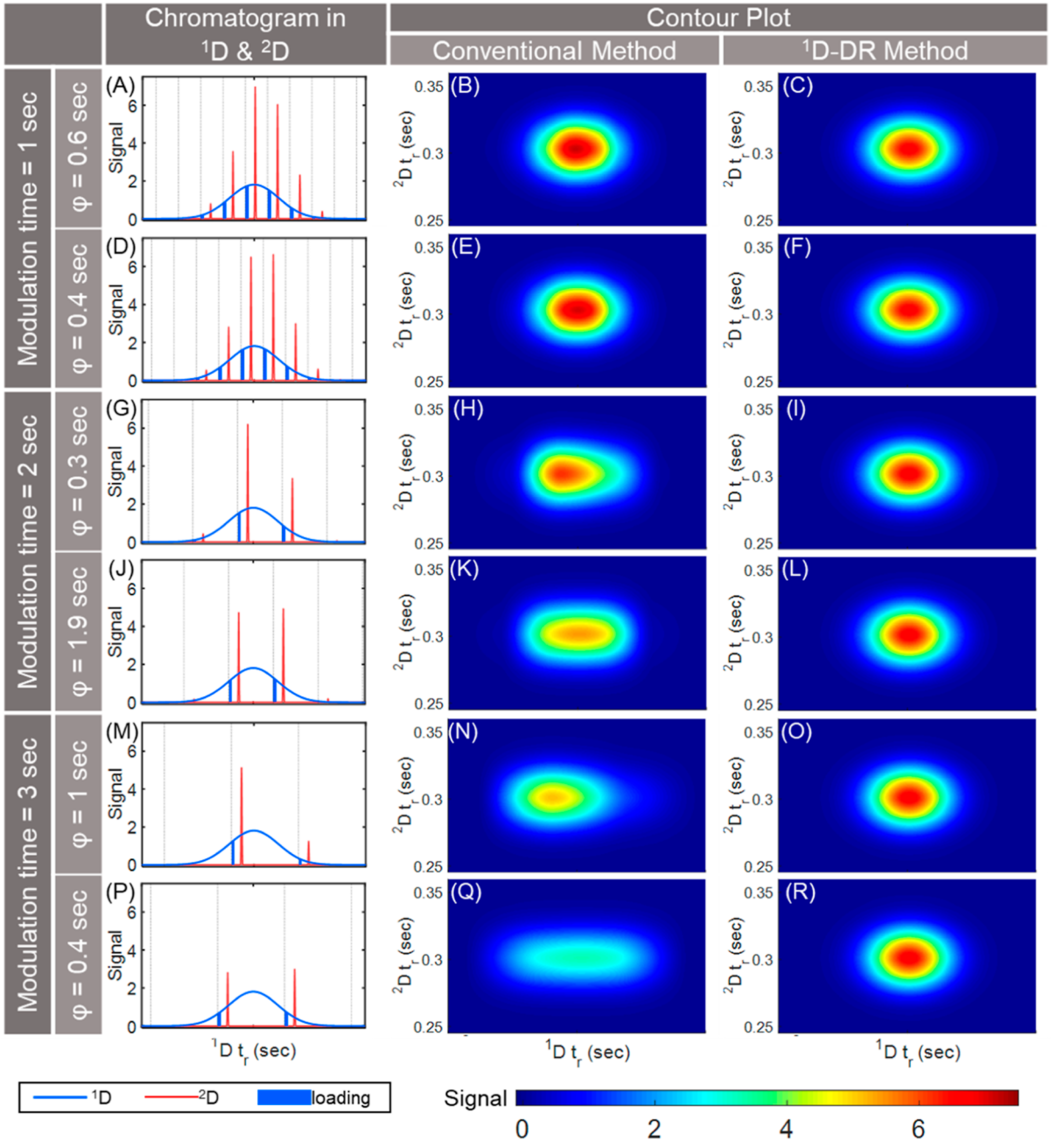

Figure 3. Artificially generated ^{1}D and ^{2}D chromatograms with reconstructed contour plots using the conventional and the ^{1}D-DR method, illustrating the influence of the modulation time (P_M) and phase shift (φ). The blue and red curves represent the ^{1}D and ^{2}D chromatograms, respectively. The blue bars mark the areas under the ^{1}D peaks during ^{1}D-to-^{2}D loading sessions. The ^{1}D and ^{2}D peak profiles are the same for all cases, with $^{1}t_r$ = 35 s, $^{2}t_r$ = 0.3 s, $^{1}W_{1/2}$ = 2.6 s, and $^{2}W_{1/2}$ = 0.035 s. Modulation time and phase shift are varied. Loading times (t_L) are kept at 0.15 s. $t_{L,pseudo}$ is set to be the same as t_L (*i.e.*, 0.15 s). The *x*-axes for all figures represent the ^{1}D retention time ranging from 30 to 40 s. More results can be found in Figure S2.

pneumatic modulation and ^{2}D separation are the same as in the μGC × μGC system described in ref 18.

RESULTS AND DISCUSSION

Influence of Modulation Time and Phase Shift. We first evaluate the influence of the modulation time and phase shift on symmetric peaks. In Figures 3 and S2, different ^{2}D chromatograms (red curves) with varied P_M (1, 2, and 3 s) are artificially generated for the same ^{1}D symmetric Gaussian peak (blue curves). For each modulation time, four ^{2}D chromatograms with different phase shifts are presented, two with in-phase modulation (φ = 0.4 and 0.9 s for P_M = 1 s; 1.9 and 0.9 s for P_M = 2 s; 0.4 and 1.9 s for P_M = 3 s), the other two with out-of-phase modulation (φ = 0.2 and 0.6 s for P_M = 1 s; 0.3 and 1.3 s for P_M = 2 s; 1 and 2.8 s for P_M = 3 s). "In-phase" and "out-of-phase" modulations refer to the modulations whose starting times are symmetrically and asymmetrically located with respect to the ^{1}D peak apex.

As can be seen from the contour plots using the conventional method (left panels in Figures 3 and S2), the in-phase modulation produces symmetric peaks while the out-of-phase modulation produces asymmetric ones (tailing in

https://doi.org/10.1021/acs.analchem.4c00202
Anal. Chem. 2024, 96, 3960−3969

Table 1. Features (Symmetry Level, ^{1}D Retention Time, Peak Volume, and Peak Width) of Reconstructed Contour Plots and the ^{1}D Peak Obtained from the ^{1}D Detector Corresponding to the Artificially Generated Peaks with Different Modulation Times P_M and Phase Shifts φ[a]

P_M (s)	φ (s)	symmetry level			^1t_r (s)			peak volume		$^1W_{1/2}$ (s)		
		Conv.	^{1}D-DR	^{1}D detector signal	Conv.	^{1}D-DR	^{1}D detector signal	Conv.	^{1}D-DR	Conv.	^{1}D-DR	^{1}D detector signal
1	0.6	lightly asymmetrical (L)	highly symmetrical	highly symmetrical	34.93	35	35	0.758	0.7	2.63	2.6	2.6
	0.4	symmetrical			35.01			0.758		2.62		
	0.2	lightly asymmetrical (R)			35.07			0.758		2.64		
	0.9	symmetrical			34.99			0.758		2.67		
2	0.3	highly asymmetrical (L)			34.35			0.752		3.23		
	1.9	symmetrical			35.07			0.750		3.72		
	1.3	highly asymmetrical (R)			35.40			0.755		2.67		
	0.9	symmetrical			34.97			0.757		2.47		
3	1	highly asymmetrical (L)			34.05			0.715		3.47		
	0.4	symmetrical			35.19			0.649		5.46		
	2.8	highly asymmetrical (R)			35.89			0.726		3.40		
	1.9	symmetrical			34.97			0.856		3.08		

[a]"L" and "R" indicate that the peak apex leans towards the left and right side, respectively. ^1t_r: ^{1}D retention time at the peak apex. Peak volume: volume under a peak in the contour plot. $^1W_{1/2}$: peak width at half-maximum of the ^{1}D projection of the peak in the contour plot.

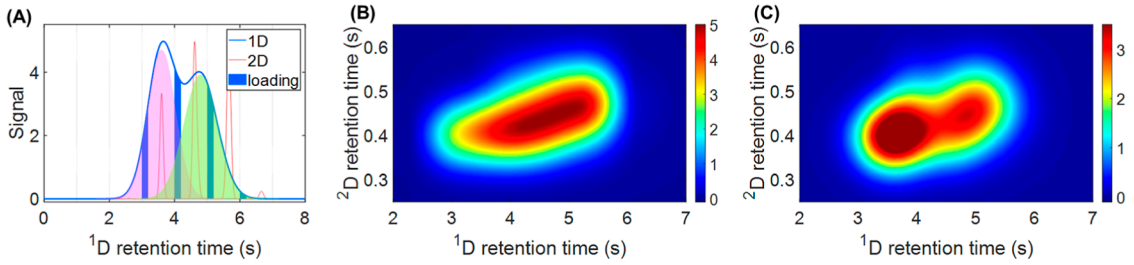

Figure 4. (A) Artificially generated ^{1}D and ^{2}D chromatograms with serious coelution issues. The blue and red curves represent the ^{1}D and ^{2}D chromatogram, respectively. The blue bars mark the areas under the ^{1}D peaks during ^{1}D-to-^{2}D loading sessions. The pink and green semiopaque areas represent two coeluted peaks eluted from ^{1}D, respectively. For the pink peak, ^1t_r = 3.6 s, ^2t_r = 0.4, $^1W_{1/2}$ = 1.0 s, and $^2W_{1/2}$ = 0.12 s. For the green peak, ^1t_r = 4.8 s, ^2t_r = 0.46 s, $^1W_{1/2}$ = 1.5 s, and $^2W_{1/2}$ = 0.15 s. t_L = 0.2 s and P_M = 1.0 s. The two analytes are partially coeluted in ^{1}D and are almost completely coeluted in ^{2}D. (B) Reconstructed contour plot with the conventional method. (C) Reconstructed contour plot using the ^{1}D-DR method.

Figure 3 and fronting in Figure S2). The increased modulation time (*i.e.*, lower modulation frequency or decreased modulation ratio, defined as the ratio between the ^{1}D peak width and P_M[23]) significantly impairs the reliability of the as-obtained contour plot with a distorted peak profile, broadened peak widths (hence increased peak volumes), and deviated ^1t_r (*i.e.*, peak apex) from its original position. Such a ^{1}D peak broadening effect can be explained by the sampling theory.[8] Therefore, using the conventional method with only the ^{2}D data inevitably reduces the overall GC × GC peak capacity and peak quantification accuracy. The detailed features (symmetry level, ^{1}D retention time ^1t_r, peak volume, and peak width) of each reconstructed pattern in the 2D contour plots are summarized in the "Conv." columns in Table 1.

In contrast, by rescaling the sequential ^{2}D data using the same ^{1}D chromatogram, the ^{1}D-DR method generates consistent contour plots with identical ^1t_r, peak volume, and peak width, as shown in the right panels of Figures 3 and S2 and summarized in the "^{1}D-DR" columns in Table 1. It should be noted that a ^{1}D detector was previously adopted in 2D assisted liquid chromatography (2DALC), along with a ^{2}D detector.[24] In that arrangement, the ^{2}D data was only used to help better resolve and hence quantify the ^{1}D peaks. In contrast, our ^{1}D-DR method is to use the ^{1}D data to fully rescale the ^{2}D chromatogram, thus correcting the entire 2D chromatogram (*i.e.*, contour plot).

More artificial experiments with asymmetric ^{1}D peaks are presented in Figure S3 and Table S1, simulating the tailing scenarios. The ^{1}D asymmetric peaks are generated using EMG and ^{2}D peaks are still symmetric Gaussian. Again, as compared to the conventional method, the ^{1}D-DR method produces more robust and consistent results.

It is worth mentioning that, in this work, when describing the analysis results as "reproducible" or "consistent", we refer in particular to the scenarios when only modulation settings vary or fluctuate, whereas all other chromatographic conditions (injections, hardware settings, and ambient environment) remain the same. Under this assumption, the effluent from the ^{1}D column before entering the modulator remains the same from run to run.

https://doi.org/10.1021/acs.analchem.4c00202
Anal. Chem. 2024, 96, 3960−3969

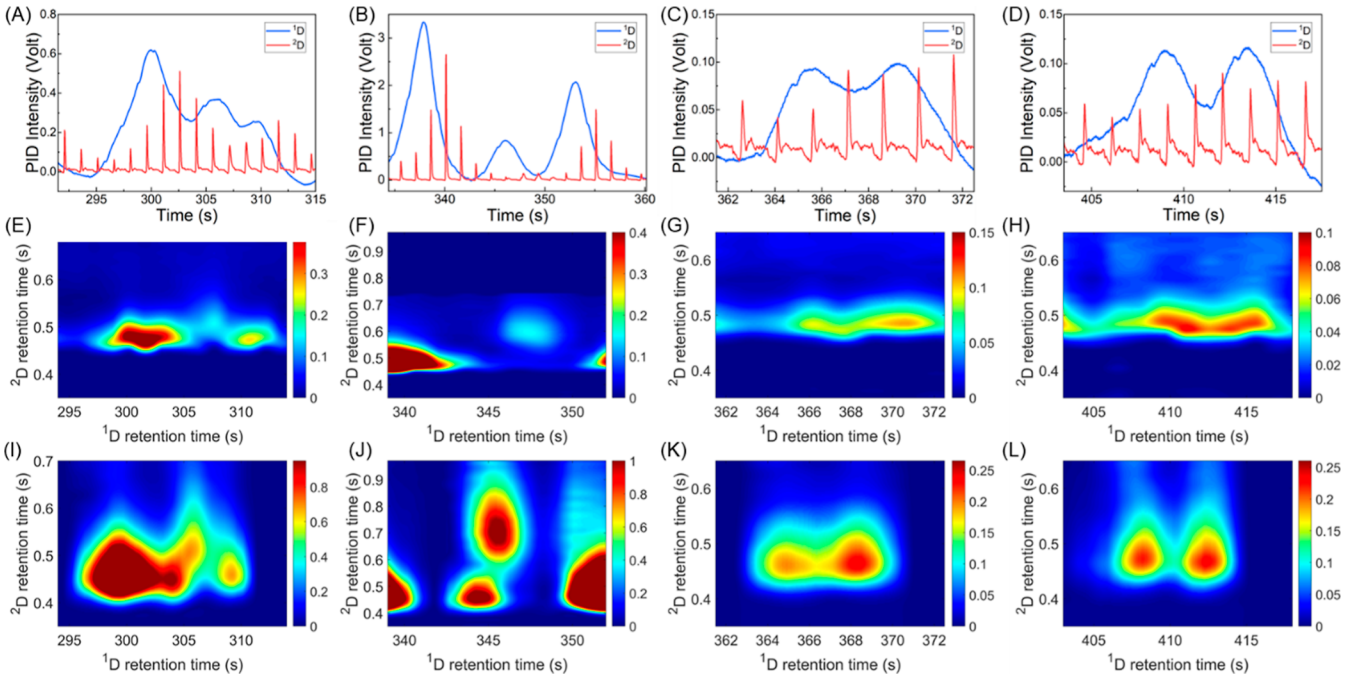

Figure 5. Portions of exemplary chromatograms of an exhaled breath sample. (A–D) ^{1}D (blue lines) and ^{2}D (red lines) chromatograms. (E–H) 2D contour plots using the conventional method [only ^{2}D data in (A–D)]. (I–L) 2D contour plots using the ^{1}D-DR method [both ^{1}D and ^{2}D data in (A–D)].

Coelution. *Artificial Data.* Figure 4 presents the artificially generated ^{1}D and ^{2}D chromatograms with serious coelution issues, as well as contour plots obtained from the conventional and the ^{1}D-DR method. Peak information in both ^{1}D and ^{2}D is detailed in the caption of Figure 4. It is shown that the reconstructed contour plot by the conventional method using the ^{2}D chromatograms alone identifies only a single peak, failing to deconvolute the coeluted peaks in the ^{1}D chromatogram. This is because the modulation (blue bars) misses to sample the peak apex or valley in the coeluted peaks, as demonstrated in Figure 4A. To further separate coeluted peaks in the contour plots, complicated deconvolution algorithms, such as the parallel factor analysis (PARAFAC)[25,26] or the Multivariate Curve Resolution-Alternating Least Squares (MCR-ALS) method,[27−29] are adopted in previous studies. But they may still not be able to completely resolve the coelution issue. In contrast, the contour plot in Figure 4C using the ^{1}D-DR method clearly shows two separated peaks, demonstrating its superior ability in handling ^{1}D coelution, which helps recover the missed peaks and hence improves the overall GC × GC peak capacity as well as peak quantification accuracy.

Experimental Data. In this work, we use an exhaled breath sample from a lab member as the model system. The portions of the ^{1}D and ^{2}D chromatograms and corresponding contour plots of the sections with noticeable performance enhancement over the conventional method are plotted in Figure 5. As compared to the conventional contour plots (Figure 5E–H), the respective plots using the new method (Figure 5I–L) produce much better resolution and sharper peaks. For example, the modulations in Figure 5A,C,D inevitably miss the peak apexes or valleys of the partially coeluted peaks, therefore the contour plots using only ^{2}D data in the conventional method waste the resolutions achieved along ^{1}D column (hence reduced resolution). Regarding the examples in Figure 5B, the conventional contour plot shows one missing peak at $^{1}t_{r}$ = 346 s, resulting from mass loss during the modulation. For example, the peak height ratio between the middle peak ($^{1}t_{r}$ = 346 s) and the neighboring peaks are ∼2:7 (the peak on the left, $^{1}t_{r}$ = 338 s) and ∼2:5 (the peak on the right, $^{1}t_{r}$ = 353 s), whereas the corresponding ratios of the ^{2}D slices after modulation decreased down to ∼1:30 and 1:20. This makes the smaller peaks between 335 and 352 s buried in the noise, and therefore, disappear in the conventional contour plot (Figure 5F). The ^{1}D-DR method is able to rescale the ^{2}D slices total area back based on the corresponding slices in ^{1}D data, thus producing one additional distinct peak (Figure 5J).

Additional work where a mixture of 40 known chemical compounds were used as the model system can be found in ref 18, showing significant improvement in resolution and quantification capabilities. All 40 peaks were separated using the ^{1}D-DR method, whereas only 32 peaks were counted in the conventional contour plot. Evaluation of individual analyte analysis was also performed with benzene and alkanes (C_{7-9}). As compared to the conventional method, values including $^{1}t_{r}$, $^{1}W_{1/2}$, and peak capacities extracted from contour plot using ^{1}D-DR method are in line with those obtained in the ^{1}D chromatogram. See detailed discussions regarding the experimental conditions in ref 18.

Duty Cycle. So far, all artificial and experimental examples in the above discussion utilize a duty cycle much smaller than 100% (mainly for pneumatic modulators). In this section, we will evaluate the performance of the ^{1}D-DR method for a duty cycle of 100% (mainly for thermal modulators, $t_{L} = P_{M}$). In Figure S4 and Table S2, we generate artificial examples with a 100% duty cycle using two different modulation times (P_{M} = 2 and 3 s), each having four different phase shifts (including in-phase, out-of-phase, symmetric, tailing, and fronting), φ. ^{1}D peak profiles, $^{2}W_{1/2}$, and $^{2}t_{r}$, are kept the same as in Figures 3 and S2, and Table 1. As shown in Figure S4, the contour plots using the conventional method deliver varied peak symmetry

https://doi.org/10.1021/acs.analchem.4c00202
Anal. Chem. 2024, 96, 3960−3969

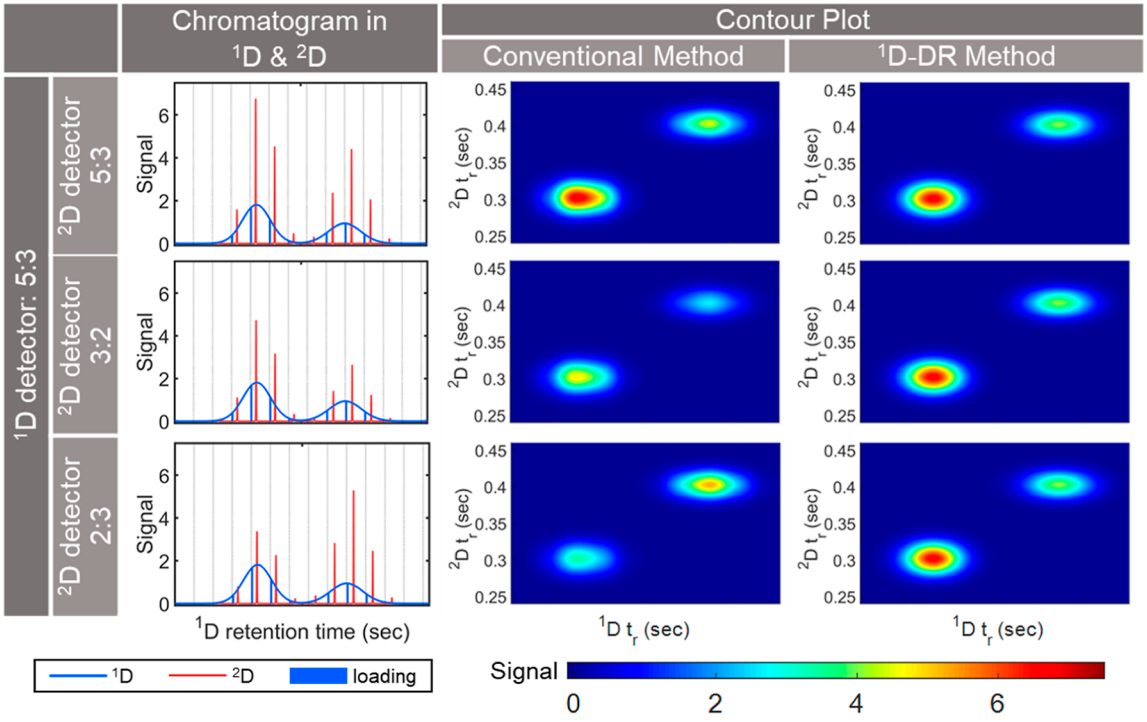

Figure 6. Artificially generated ^{1}D and ^{2}D chromatograms with different ^{1}D and ^{2}D detector responsivity ratios and their corresponding reconstructed contour plots using the conventional method and the ^{1}D-DR method. The *x*-axes for all figures represent the ^{1}D retention time ranging from 30 to 50 s.

levels, ^1t_r, and $^1W_{1/2}$ (hence varied peak capacity). Regarding the ^{1}D-DR method with $t_{L,pseudo}$ set as t_L (*i.e.*, P_M), identical contour plots, ^1t_r, peak volumes, and $^1W_{1/2}$ are obtained regardless of the phase shift (Table S2). The ^1t_r values obtained from the ^{1}D-DR contour plot are identical to the values extracted directly from the ^{1}D detector signal.

$^1W_{1/2}$ from a contour plot using ^{1}D-DR is generally smaller than that from the conventional method (hence improving peak capacity). However, we do notice that $^1W_{1/2}$ from the ^{1}D-DR contour plot, though consistent among various phase shift values, are higher than the value directly extracted from the ^{1}D detector signal. This is because as compared to a pneumatic modulator ($t_L \ll {}^1W_{1/2}$), t_L is much wider (the duty cycle is close or equal to 100%) in a thermal modulator and the increased t_L leads to the peak broadening in step 2C in the ^{1}D-DR method. If a better resolution is desired (that is, $^1W_{1/2}$ decreases to the value that is the same as obtained directly from the ^{1}D detector signal), one can set the value of $t_{L,pseudo}$ in eq 5 to be much smaller than t_L and $^1W_{1/2}$. For example, in Figure S5 when we decrease $t_{L,pseudo}$ in step 2C from 2 or 3 s to 0.15 s (same values as in Figures 3 and S2 and Table 1), identical contour plots are obtained regardless of P_M and φ. The as-obtained contour plots, together with ^1t_r, $^1W_{1/2}$, symmetric level, are the same as in Figures 3 and S2 and Table 1 and as the corresponding values extracted from the ^{1}D signal, although a 100% duty cycle is used.

Figures S6 and S7 systematically investigate the influence of the phase shift on a challenging case with a duty cycle = 100%, where two sharp peaks are seriously coeluted in both dimensions. A large modulation time P_M (=2 s) is intentionally selected, which is bigger than $^1W_{1/2}$ of both coeluted peaks (1 and 1.2 s) and the distance between the two peak apexes (1.8 s). All possible phase shifts distanced by 0.1 s (φ = 0−1.9 s) are enumerated in Figure S6(A1−T1). Figure S6(A2−T2) show the corresponding contour plots using the conventional method. These 20 contour plots vary drastically and half of them fail to resolve the coeluted peaks (Figure S6(A2−F2,J2,K2)). Although Figure S6(M2−T2) completely resolve the coeluted peaks, the retention time, ^1t_r, for both peaks shifts substantially, which may affect the subsequent identification of these peaks.

The contour plot using the ^{1}D-DR method, with $t_{L,pseudo}$ set as P_M = 2 s, continues to exhibit high consistency by yielding identical contour plots (Figure S7A). However, it does not show better performance in terms of resolution, that is, the two ^{1}D peaks are not well resolved. This is because $t_{L,pseudo}$, being set as 2 s (=P_M) is too wide, which inevitably covers the entire peak apex or even both peak apexes and the peak valley. Consequently, $^1A_k = \int_{t_k}^{t_k+t_{L,pseudo}} {}^1S(t)\,dt$ changes in a less distinct way when shifting the pseudoloading session from k to k + 1. Therefore, the resolution achieved in ^{1}D (by using a ^{1}D detector) is not fully utilized. In contrast, when we reduce $t_{L,pseudo}$ to 0.1 s (≪peak width and distance between the peak apexes), a contour plot (Figure S7B) with well-resolved ^{1}D peaks, and correct and consistent ^1t_r and peak volumes are produced, regardless of the phase shift. The above discussion shows that the ^{1}D-DR method has performance superior to the conventional method, even for a duty cycle of 100%, in which case one can improve the resolution by setting $t_{L,pseudo}$ to be much smaller than the ^{1}D peak width (*e.g.*, ∼10 times smaller than $^1W_{1/2}$), especially when the modulation time is large compared the peak widths and distance between neighboring peak apexes.

Versatility in Detector Responsivity. Another advantage of using the ^{1}D chromatogram data to rescale the contour plot is that it makes the reconstructed contour plots immune to detector responsivity changes. Up until now, we have assumed

https://doi.org/10.1021/acs.analchem.4c00202
Anal. Chem. 2024, 96, 3960−3969

that ^{1}D and ^{2}D detectors are identical. In real-world scenarios, the ^{1}D and ^{2}D detectors may have different responsivities even to the same analyte (such as photoionization detector—PID for ^{1}D, and flame ionization detector—FID for ^{2}D). To demonstrate the robustness of the ^{1}D-DR method with varying responsivity ratios between the ^{1}D and ^{2}D detectors, three scenarios with different ^{1}D and ^{2}D detector responsivity ratios were generated as shown in Figure 6 and Table S3. Other than the responsivity ratios, all the other peak features were kept the same for the three scenarios.

In our modeling, the ^{1}D detector has a responsivity 5 and 3 to species A and B, respectively. In the first row of Figure 6, we assume that the ^{2}D detector is of the same type as the ^{1}D detector and therefore has the responsivity of 5 and 3 to species A and B, too. Note the absolute responsivity of the ^{2}D detector changes proportionately (for example, responsivity to species A and B increases to 10 and 6), it does not change the 2D contour plot and the results due to the ratiometric nature between the ^{1}D and ^{2}D detection of our method (see eqs 3 and 8). This row is used as a control, where both the conventional and our method can see two peaks in the 2D contour plot with accurate quantification (or peak volume).

The second row simulates the scenarios where the ^{1}D and ^{2}D detectors have different responsivities to species A and B, but both ^{1}D and ^{2}D have a higher responsivity to species A than to species B (*i.e.*, ^{1}D detector has responsivity of 5 and 3 to species A and B, respectively, whereas ^{2}D detector has a responsivity of 3 and 2 to species A and B, respectively). The third row simulates the scenario where the ^{2}D detector has a responsivity of 2 to species A, lower than its responsivity (=3) to species B. In both scenarios, the conventional method yields peaks with different peak volumes and width, whereas our method yields consistent peak features. This is because all the changes in the contour plots due to the ^{2}D detector ratio change are rescaled according to the original ^{1}D detector responsivity ratio. Our method enables high versatility in detector selection. For example, we can choose PID/PID as the ^{1}D and ^{2}D detectors, or PID/FID as the ^{1}D and ^{2}D detectors.

Furthermore, the above discussion also suggests that we can afford some mass loss in the ^{1}D detector. In our previous discussion, we had assumed that the ^{1}D detector is nondestructive. But now, based on our results in Figure 6, we can use a ^{1}D detector that may have some mass loss (*i.e.*, minimally destructive detector rather than nondestructive detector). The mass loss scenario can be understood as ^{1}D and ^{2}D showing different responsivities. For example, with a 10% mass loss, the absolute responsivity of ^{1}D and ^{2}D detector becomes 5:3 *vs* 4.5:2.7 (for the first row in Figure 6) and 5:3 *vs* 2.7:1.8 (for the second row in Figure 6). The scaling factor introduced by the mass loss can be easily corrected after rescaling with the ^{1}D data, as long as the mass loss is not too high to hide all ^{2}D signals below the baseline noise level.

CONCLUSIONS

In conclusion, by leveraging a ^{1}D detector, we have developed a novel ^{1}D-guided differential rescaling algorithm using the ^{1}D data that can significantly improve GC × GC performance in terms of chromatographic resolution (or peak capacity), retention time accuracy, and quantification precision. We showed that our new method exhibits high stability and consistency against the influence of modulation time selection and phase shift fluctuation, the presence of ^{1}D coelution, and ^{1}D/^{2}D detector responsivity changes. The method can easily be extended to other multidimensional instruments such as LC × LC. One of the major drawbacks of the proposed method is added complexity in instruments due to the extra detector, which may be overcome by integrating the detector with the column during future device development.

ASSOCIATED CONTENT

Supporting Information

The Supporting Information is available free of charge at https://pubs.acs.org/doi/10.1021/acs.analchem.4c00202.

^{1}D-guided differential rescaling method and the influence of modulation time, phase shift, duty cycle, and pseudoloading time on 2D contour plots, figures compare the 2D contour plots generated with the conventional method and the ^{1}D-guided differential rescaling method, and tables summarize the parameters and results used in the aforementioned figures. (PDF)

AUTHOR INFORMATION

Corresponding Author

Xudong Fan − *Department of Biomedical Engineering, University of Michigan, Ann Arbor, Michigan 48109, United States; Center for Wireless Integrated MicroSensing and Systems (WIMS^2) and Max Harry Weil Institute for Critical Care Research and Innovation, University of Michigan, Ann Arbor, Michigan 48109, United States;* orcid.org/0000-0003-0149-1326; Email: xsfan@umich.edu

Authors

Wenzhe Zang − *Department of Biomedical Engineering, University of Michigan, Ann Arbor, Michigan 48109, United States; Center for Wireless Integrated MicroSensing and Systems (WIMS^2) and Max Harry Weil Institute for Critical Care Research and Innovation, University of Michigan, Ann Arbor, Michigan 48109, United States;* orcid.org/0000-0003-2203-4634

Xiaheng Huang − *Department of Biomedical Engineering, University of Michigan, Ann Arbor, Michigan 48109, United States; Center for Wireless Integrated MicroSensing and Systems (WIMS^2), Max Harry Weil Institute for Critical Care Research and Innovation, and Department of Electrical Engineering and Computer Science, University of Michigan, Ann Arbor, Michigan 48109, United States;* orcid.org/0000-0002-0960-1211

Ruchi Sharma − *Department of Biomedical Engineering, University of Michigan, Ann Arbor, Michigan 48109, United States; Center for Wireless Integrated MicroSensing and Systems (WIMS^2) and Max Harry Weil Institute for Critical Care Research and Innovation, University of Michigan, Ann Arbor, Michigan 48109, United States;* orcid.org/0000-0002-3604-9784

Complete contact information is available at: https://pubs.acs.org/10.1021/acs.analchem.4c00202

Notes

The authors declare no competing financial interest.

ACKNOWLEDGMENTS

The authors acknowledge the support from National Institute for Occupational Safety and Health (NIOSH) *via* R01 OH011082-01A1 and the Office of the Director of National

Intelligence (ODNI), Intelligence Advanced Research Projects Activity (IARPA) *via* IARPA FA8650-19-C-9101. The views and conclusions contained herein are those of the authors and should not be interpreted as necessarily representing the official policies or endorsements, either expressed or implied, of the ODNI, IARPA, or the U.S. Government. The U.S. Government is authorized to reproduce and distribute reprints for Governmental purposes notwithstanding any copyright annotation thereon.

REFERENCES

(1) Zanella, D.; Focant, J. F.; Franchina, F. A. *Anal. Sci. Adv.* **2021**, *2*, 213−224.
(2) Mondello, L.; Tranchida, P. Q.; Dugo, P.; Dugo, G. *Mass Spectrom. Rev.* **2008**, *27*, 101−124.
(3) Milani, N. B.; van Gilst, E.; Pirok, B. W.; Schoenmakers, P. J. *J. Sep. Sci.* **2023**, *46*, 2300304.
(4) Adcock, J. L.; Adams, M.; Mitrevski, B. S.; Marriott, P. J. *Anal. Chem.* **2009**, *81*, 6797−6804.
(5) Marriott, P.; Shellie, R. *TrAC, Trends Anal. Chem.* **2002**, *21*, 573−583.
(6) Ong, R. C. Y.; Marriott, P. J. *J. Chromatogr. Sci.* **2002**, *40*, 276−291.
(7) Boswell, H.; Chow, H. Y.; Gorecki, T. Chapter 4—Modulators. In *Separation Science and Technology*; Snow, N. H., Ed.; Academic Press, 2020; Vol. *12*, pp 89−140.
(8) Blumberg, L. M.; David, F.; Klee, M. S.; Sandra, P. *J. Chromatogr. A* **2008**, *1188*, 2−16.
(9) Murphy, R. E.; Schure, M. R.; Foley, J. P. *Anal. Chem.* **1998**, *70*, 1585−1594.
(10) Khummueng, W.; Harynuk, J.; Marriott, P. J. *Anal. Chem.* **2006**, *78*, 4578−4587.
(11) Blumberg, L. M. *Temperature-Programmed Gas Chromatography*; John Wiley & Sons, 2010.
(12) Zhu, Z.; Harynuk, J.; Górecki, T. *J. Chromatogr. A* **2006**, *1105*, 17−24.
(13) Harynuk, J.; Górecki, T.; Zeeuw, J. d. *J. Chromatogr. A* **2005**, *1071*, 21−27.
(14) Nolvachai, Y.; McGregor, L.; Spadafora, N. D.; Bukowski, N. P.; Marriott, P. J. *Anal. Chem.* **2020**, *92*, 12572−12578.
(15) Zhu, H.; Nidetz, R.; Zhou, M.; Lee, J.; Buggaveeti, S.; Kurabayashi, K.; Fan, X. *Lab Chip* **2015**, *15*, 3021−3029.
(16) Wei-Hao Li, M.; Ghosh, A.; Venkatasubramanian, A.; Sharma, R.; Huang, X.; Fan, X. *ACS Sens.* **2021**, *6*, 2348−2355.
(17) Lee, J.; Zhou, M.; Zhu, H.; Nidetz, R.; Kurabayashi, K.; Fan, X. *Anal. Chem.* **2016**, *88*, 10266−10274.
(18) Huang, X.; Li, M. W.-h.; Zang, W.; Huang, X.; Sivakumar, A. D.; Sharma, R.; Fan, X. *Microsyst. Nanoeng.* **2022**, *8*, 115.
(19) Allen, R. C.; Rutan, S. C. *Anal. Chim. Acta* **2011**, *705*, 253−260.
(20) Akima, H. *J. ACM* **1970**, *17*, 589−602.
(21) Sharma, R.; Zang, W.; Tabartehfarahani, A.; Lam, A.; Huang, X.; Sivakumar, A. D.; Thota, C.; Yang, S.; Dickson, R. P.; Sjoding, M. W.; et al. *JAMA Netw. Open* **2023**, *6*, No. e230982.
(22) Sharma, R.; Zang, W.; Zhou, M.; Schafer, N.; Begley, L. A.; Huang, Y. J.; Fan, X. *Metabolites* **2021**, *11* (5), 265.
(23) Marriott, P. J.; Mühlen, C. v. *Sci. Chromatogr.* **2016**, *8*, 7−23.
(24) Cook, D. W.; Rutan, S. C.; Stoll, D. R.; Carr, P. W. *Anal. Chim. Acta* **2015**, *859*, 87−95.
(25) Bro, R. *Chemometr. Intell. Lab. Syst.* **1997**, *38*, 149−171.
(26) Pierce, K. M.; Kehimkar, B.; Marney, L. C.; Hoggard, J. C.; Synovec, R. E. *J. Chromatogr. A* **2012**, *1255*, 3−11.
(27) Bailey, H. P.; Rutan, S. C. *Chemometr. Intell. Lab. Syst.* **2011**, *106*, 131−141.
(28) Tauler, R.; Smilde, A.; Kowalski, B. *J. Chemometr.* **1995**, *9*, 31−58.
(29) Matos, J. T. V.; Duarte, R. M. B. O.; Duarte, A. C. *J. Chromatogr. B* **2012**, *910*, 31−45.

https://doi.org/10.1021/acs.analchem.4c00202
Anal. Chem. 2024, 96, 3960−3969